

Moderate Steepening of Galaxy Cluster Dark Matter Profiles by Baryonic Pinching

Jesper Sommer-Larsen^{1,2*} & Marceau Limousin^{3,1*}

¹*Dark Cosmology Centre, Niels Bohr Institute, University of Copenhagen, Juliane Maries Vej 30, DK-2100 Copenhagen, Denmark*

²*Excellence Cluster Universe, Technische Universität München, Boltzmannstrasse 2, 85748 Garching, Germany*

³*Laboratoire d’Astrophysique de Marseille, UMR 6610, CNRS-Université de Provence, 38 rue Frédéric Joliot-Curie, 13388 Marseille Cedex 13, France*

Accepted 2009 August 31. Received 2009 August 30; in original form 2009 June 3

ABSTRACT

To assess the effect of baryonic “pinching” of galaxy cluster dark matter (DM) haloes, cosmological (Λ CDM) TreeSPH simulations of the formation and evolution of two galaxy clusters have been performed, with and without baryons included.

The simulations with baryons invoke star formation, chemical evolution with non-instantaneous recycling, metallicity dependent radiative cooling, strong star-burst, driven galactic super-winds and the effects of a meta-galactic UV field, including simplified radiative transfer. The two clusters have $T \simeq 3$ and 6 keV, respectively, and, at $z \sim 0$, both host a prominent, central cD galaxy.

Comparing the simulations without and with baryons, it is found for the latter that the inner DM density profiles, $r \lesssim 50$ -100 kpc, steepen considerably: $\Delta\alpha \sim 0.5$ -0.6, where $-\alpha$ is the logarithmic DM density gradient. This is primarily due to the central stellar cDs becoming very massive, as a consequence of the onset of late time cooling flows and related star formation. Once these spurious cooling flows have been corrected for, and the cluster gravitational potentials dynamically adjusted, much smaller pinching effects are found: $\Delta\alpha \sim 0.1$. Including the effects of baryonic pinching, central slopes of $\alpha \simeq 1.0$ and 1.2 are found for the DM in the two clusters, interestingly close to recent observational findings for galaxy cluster Abell 1703 based on strong gravitational lensing.

For the simulations with baryons, the inner density profile of DM and cluster gas (ICM) combined is found to be only very marginally steeper than that of the DM, $\Delta\alpha \lesssim 0.05$. However, the total matter inner density profiles are found to be $\Delta\alpha \sim 0.5$ steeper than the inner profiles in the dark matter only simulations.

Key words: cosmology: theory — cosmology: numerical simulations — galaxies: clusters — galaxies: formation — galaxies: evolution

1 INTRODUCTION

Large N-body cosmological simulations have been carried out for a decade, with the goal of making statistical predictions on dark matter (DM) halo properties. Because of numerical issues, most of these large cosmological simulations contain dark matter particles only. They all reliably predict that the 3D density profile $\rho_{\text{DM}}(r)$ should fall as r^{-3} at large radii (but within the virial radius). Observations have confirmed these predictions for cluster sized haloes (*e.g.* Kneib et al. 2003; Pointecouteau et al. 2005; Mandelbaum et al. 2008; Okabe et al. 2009). This agreement

is likely to be connected with the fact that at large radius, the density profile of a galaxy cluster is dark matter dominated and the influence of baryons can be neglected. On smaller scales, parameterizing the 3D density profile of the DM using a cuspy profile $\rho_{\text{DM}} \propto r^{-\alpha}$; dark matter only simulations predict a logarithmic slope $\alpha \sim 1$ -1.5 for $r \rightarrow 0$. The exact value of the central slope and its universality is debated (Navarro et al. 1997; Moore et al. 1998; Ghigna et al. 2000; Ricotti 2003; Navarro et al. 2004; Gao et al. 2008). Theoretical efforts indicate that the inner logarithmic slope of DM halos should be $\alpha \sim 0.8$ (Austin et al. 2005; Hansen & Stadel 2006). Although clearly of interest, these dark matter only studies and their predictions do not help much to make comparison with observations. Indeed, observing the central part (*i.e.* the inner ~ 500 kpc) of a galaxy

* E-mail: jslarsen@astro.ku.dk (JSL); marceau.limousin@oamp.fr (ML)

cluster at any wavelength reveals the presence of baryons (in the forms of stars and X-ray emitting hot gas). Thus any attempt to compare observations to simulations in the center of galaxy clusters has to be made with numerical simulations (or calculations) taking into account the baryonic component and its associated physics.

On the numerical side, efforts are currently being made to include effects of baryons in a realistic way in the simulations (see below). Problems remain, however: for example, due to the so-called “over-cooling problem”, numerical simulations tend to predict central brightest cluster galaxies which are too blue and too massive relative to observations. Different effects do compete when it comes to the central slope of the density profile: the cooling of gas in the central regions of galaxies and clusters is expected to lead to a more concentrated dark matter distribution (the so-called adiabatic contraction, see Blumenthal et al. 1986; Gnedin et al. 2004; Gustafsson et al. 2006). On the other hand, dynamical friction heating of massive galaxies against the diffuse cluster dark matter could in principle flatten the slope of the DM density profile (El-Zant et al. 2001; Nipoti et al. 2003, 2004; Ma & Boylan-Kolchin 2004). Also, the properties of the inner part of simulated galaxy clusters (even in dark matter only simulations) can depend significantly on initial conditions as demonstrated in Kazantzidis et al. (2004). Consequently, no coherent picture has yet emerged from N-body simulations when it comes to the shape of the inner density profile of structures.

On the observational side, efforts have been put on probing the central slope α of the underlying dark matter distribution. These analyzes have led to wide-ranging results, whatever the method used: X-ray (Ettori et al. 2002; Arabadjijs et al. 2002; Lewis et al. 2003; Zappacosta et al. 2006); lensing (Tyson et al. 1998; Smith et al. 2001; Dahle et al. 2003; Sand et al. 2002; Gavazzi et al. 2003; Gavazzi 2005; Sand et al. 2004, 2008; Bradač et al. 2007; Limousin et al. 2008; Richard et al. 2009; Oguri et al. 2009) or dynamics (Kelson et al. 2002; Biviano & Salucci 2006). This highlights the difficulty of such studies and the possible large scatter in the value of α from one cluster to another.

In summary, one needs to probe observationally and numerically the behavior of the *underlying* dark matter distribution (i.e. after the baryonic component has been separated from the dark matter component) in the central parts of galaxy clusters. The main difficulties are: i) Observationally, to be able to disentangle the baryonic component and the underlying dark matter distribution; ii) Numerically, to implement the baryonic physics into the simulations; iii) Then to compare both approaches in a consistent way.

Sand et al. (2002, 2004, 2008) carried out lensing analyzes aiming to probe the central mass distribution in six galaxy clusters, using the measured velocity dispersion profile of the cD galaxy as an extra constrain. They found central density slopes smaller than 1.

Recently, there have been a growing interest on Abell 1703, a massive $z = 0.28$ (Allen et al. 1992) X-ray cluster with a luminosity $L_x = 8.7 \times 10^{44} \text{ erg s}^{-1}$ (Böhringer et al. 2000). It contains a large number of gravitational arcs, enabling a very detailed lensing analysis. Moreover, although it displays an intriguing filamentary structure along the north-south direction, it looks rather circular from the geometrical configuration of its multiply

imaged systems, in particular its giant arc, located at large angular separation ($\sim 35'' \sim 147 \text{ kpc}$). It is a uni-modal cluster, likely to be relaxed and characterized by a central dominant elliptical cD galaxy. This makes it much easier to interpret the results of the modeling compared to bi-modal clusters such as Abell 1689 (Limousin et al. 2007b; Riemer-Sørensen et al. 2009), Abell 2218 (Elíasdóttir et al. 2007), Abell 68 (Richard et al. 2007) or MS 2053.7-0449 (Verdugo et al., 2007). In fact, regular relaxed clusters are rare at such redshifts (Smith et al. 2005). Finally, it displays a remarkable lensing configuration, forming a central “ring” composed of four bright images that represent a rare example of lensing by a hyperbolic umbilic catastrophe (Orban de Xivry & Marshall 2009). This ring is located close to the central cD galaxy ($4.9''$, corresponding to 17-38 kpc), providing a robust constraint in the very central part of the cluster.

This motivated several lensing works on Abell 1703 aimed to probe the dark matter density slope of the central region ($\sim 20 - 200 \text{ kpc}$), modeling the dark matter distribution of Abell 1703 by a generalized NFW profile, viz.

$$\rho(r) = \frac{\rho_c \delta_c}{(r/r_s)^{\alpha_{NFW}} (1 + (r/r_s))^{3-\alpha_{NFW}}}, \quad (1)$$

where r_s is the scale radius. These works (Limousin et al. 2008; Saha et al. 2009; Richard et al. 2009; Oguri et al. 2009) determined the inner slope α_{NFW} to be consistent with the universal profile ($\alpha_{NFW} = 1$). The more recent strong lensing analysis by Richard et al (2009), based on the identification of 16 multiply imaged systems, of which 10 are spectroscopically confirmed, found $\alpha_{NFW} = 0.92 \pm 0.04$ (1σ confidence level). Note that the scale radius derived by Richard et al (2009) is found in agreement with that found by Oguri et al (2009) when combining strong and weak lensing. Since the scale radius needs weak lensing data to be properly constrained, this is important given the degeneracies arising between the scale radius and the inner slope.

Assuming that pure dark matter haloes are well described by the standard NFW profile with $\alpha_{NFW} = 1$, the indication of the above results on Abell 1703 is that the baryonic pinching of the dark matter halo, probably mainly caused by the central dominant cD galaxy, does not substantially affect the dark matter density slope in the central region of the cluster.

On the theoretical/numerical front it has only recently been possible to carry out fully cosmological gas-dynamical/N-body simulations of the formation and evolution of galaxy clusters at a sufficient level of numerical resolution and physical sophistication that the cool-out of gas, star-formation, chemical evolution and gas inflows and outflows related to individual cluster galaxies can be modeled to a reasonable degree of realism (e.g., Kay et al. 2002; Thomas et al. 2002; Valdarnini 2003; Tornatore et al. 2004; Sommer-Larsen et al. 2005; D’Onghia et al. 2005; Romeo et al. 2005, 2006; Saro et al. 2006; Muanwong et al. 2006; Tornatore et al. 2007; Romeo et al. 2008).

Romeo et al. (2005), Romeo et al. (2006), D’Onghia et al. (2005) and Sommer-Larsen et al. (2005) presented fully cosmological simulations of galaxy groups and clusters. The TreeSPH code used was building on the code used for simulating galaxy formation (e.g., Sommer-Larsen, Götz & Portinari 2003), improved to

include modeling of non-instantaneous chemical evolution (Lia, Portinari & Carraro 2002a), metallicity-dependent, atomic radiative cooling, strong supernova, and (optionally) AGN, driven galactic winds and thermal conduction. The two clusters simulated have $z=0$ virial masses $M_{vir} \sim 3 \times 10^{14}$ and $1.2 \times 10^{15} M_{\odot}$, one approximately the size of the Virgo cluster and the other of the Coma cluster. They were both selected to be fairly relaxed, and both display central prominent cD galaxies at $z=0$ as well as at $z=0.28$. In this paper we reanalyze the simulations of the two clusters with emphasis on the dark matter density profiles. We also present re-simulations of the clusters aimed at correcting for the effects of spurious, late time cooling-flows. Finally, we present results of new simulations of the *same* two clusters, identical to the previous ones except that they were carried out with dark matter only. We then compare the results of simulations with and without baryons, to quantify the effects of baryons (especially the cDs) on galaxy cluster dark matter profiles.

The paper is organized as follows: the code and the simulations are described in section 2, the results obtained are presented in section 3 and discussed in section 4, and, finally, section 5 constitutes the conclusion.

Throughout the paper a Λ CDM cosmology with $\Omega_M = 0.3$, $\Omega_{\Lambda} = 0.7$ and a Hubble constant $H_0 = 70 \text{ km s}^{-1} \text{ Mpc}^{-1}$ is assumed.

2 THE CODE AND SIMULATIONS

The code used for the simulations is a significantly improved version of the TreeSPH code we have used previously for galaxy formation simulations (Sommer-Larsen, Götz & Portinari 2003): Full details on the code are given in Romeo et al. (2006); here we recall the main improvements over the previous version. (1) In lower resolution regions (which will always be present in cosmological CDM simulations) an improvement in the numerical accuracy of the integration of the basic equations is obtained by solving the entropy equation rather than the thermal energy equation — we have adopted the “conservative” entropy equation solving scheme suggested by Springel & Hernquist (2002). (2) Cold high-density gas is turned into stars in a probabilistic way as described in Sommer-Larsen, Götz & Portinari (2003). In a star-formation event an SPH particle is converted fully into a star particle. Non-instantaneous recycling of gas and heavy elements is described through probabilistic “decay” of star particles back to SPH particles as discussed by Lia, Portinari & Carraro (2002a). In a decay event a star particle is converted fully into an SPH particle. (3) Non-instantaneous chemical evolution tracing 10 elements (H, He, C, N, O, Mg, Si, S, Ca and Fe) has been incorporated in the code following Lia et al. (2002a,b); the algorithm includes supernovæ of type II and type Ia, and mass loss from stars of all masses. Metal diffusion in Lia et al. was included with a diffusion coefficient κ derived from models of the expansion of individual supernova remnants. A much more important effect in the present simulations, however, is the redistribution of metals (and gas) by means of star-burst driven “galactic super-winds” (see point 5). This is handled self-consistently by the code, so we set $\kappa=0$ in the present

simulations. (4) Atomic radiative cooling depending both on the metal abundance of the gas and on the meta-galactic UV field, modeled after Haardt & Madau (1996) is invoked. We also include a simplified treatment of radiative transfer, by switching off the UV field where the gas becomes optically thick to Lyman limit photons on scales of ~ 1 kpc. (5) Star-burst driven, galactic super-winds are incorporated in the simulations. This is required to expel metals from the galaxies and get the abundance of the ICM to the observed level of about 1/3 solar in iron. A burst of star formation is modeled in the same way as the “early bursts” of Sommer-Larsen, Götz & Portinari (2003), i.e. by halting cooling in the surrounding gas particles, to mimic the initial heating and subsequent adiabatic expansion phase of the super-shell powered by the star-burst; this scheme ensures effective energy coupling and feedback between the bursting star particle and the surrounding gas. The strength of the super-winds is modeled through a free parameter f_{wind} which determines how large a fraction of the new-born stars partake in such bursting, super-wind driving star formation. We find that in order to get an iron abundance in the ICM comparable to observations, $f_{wind} \gtrsim 0.5$ and at the same time a fairly top-heavy Initial Mass Function (IMF) has to be used. (6) Thermal conduction was implemented in the code following Cleary & Monaghan (1999).

In this paper we present results for two simulated clusters, “Virgo” and “Coma”. Both systems were chosen to be fairly relaxed (no $\gtrsim 1:2$ merging at $z \lesssim 1$). Virial masses at $z=0$ are approximately 2.0×10^{14} and $8.7 \times 10^{14} h^{-1} M_{\odot}$ and X-ray emission weighted temperatures 3.0 and 6.0 keV, respectively. The clusters were selected from a cosmological, DM-only simulation of a flat Λ CDM model, with $\Omega_M=0.3$, $\Omega_b=0.036$, $h=0.7$ and $\sigma_8=0.9$ and a box-length of $150 h^{-1} \text{ Mpc}$. Mass and force resolution was increased in, and gas particles added to, Lagrangian regions enclosing the clusters. The Virgo cluster was then re-simulated using 2.3 million baryonic+DM particles with $m_{gas}=m_* = 3.1 \times 10^7$ and $m_{DM}=2.3 \times 10^8 h^{-1} M_{\odot}$ for the high resolution gas, star and dark matter particles. Gravitational (spline) softening lengths of $\epsilon_{gas}=\epsilon_* = 1.4$ and $\epsilon_{DM}=2.7 h^{-1} \text{ kpc}$, respectively, were adopted. The more massive Coma cluster was re-simulated using 1.0 million baryonic+DM particles with $m_{gas}=m_* = 2.5 \times 10^8$ and $m_{DM}=1.8 \times 10^9 h^{-1} M_{\odot}$, $\epsilon_{gas}=\epsilon_* = 2.8$ and $\epsilon_{DM}=5.4 h^{-1} \text{ kpc}$. As a resolution test, the Virgo cluster was also simulated at this (eight times lower) mass and (two times lower) force resolution. This simulation will be denoted “VirgoLR”.

For all simulations, gravitational softening lengths were fixed in co-moving coordinates till $z=6$, subsequently in physical coordinates.

For the simulation presented in this paper $f_{wind}=0.8$, and an Arimoto-Yoshii IMF (of slope $x=-1$, shallower than the Salpeter slope $x=-1.35$) with mass limits $[0.1-100] M_{\odot}$ was adopted. AGN driven winds were not invoked. Moreover, the thermal conductivity was set to zero assuming that thermal conduction in the ICM is highly suppressed by magnetic fields (e.g., Ettori & Fabian 2000). We note, that in relation to all relevant quantities presented in this paper, no significant difference is found between simulations with zero thermal conductivity and simulations invoking thermal conduction at 1/3 of the Spitzer level (Romeo et al. 2005).

Table 1. Numerical and physical characteristics of the cluster simulations: mass of DM/gas/star particles and the respective gravitational (spline) softening lengths; total number of particles and initial redshift of each run; virial mass, radius and temperature of simulated clusters (last three columns, referring to $z=0$).

run	m_{DM}	m_{gas} [$10^7 M_{\odot}/h$]	m_*	ϵ_{DM}	ϵ_{gas} [kpc/h]	ϵ_*	N_{tot}	z_i	M_{vir} [$10^{14} M_{\odot}$]	R_{vir} [Mpc]	kT [keV]
Coma	180	25	25	5.4	2.8	2.8	950000	19	12.4	2.9	6
Virgo	23	3.1	3.1	2.7	1.4	1.4	2235000	39	2.8	1.7	3
VirgoLR	180	25	25	5.4	2.8	2.8	260000	19	2.8	1.7	3
ComaDM	26	-	-	2.8	-	-	4000000	39	12.4	2.9	-
VirgoDM	26	-	-	2.8	-	-	1200000	39	2.8	1.7	-

2.1 Correcting for the effects of late quasi-stationary cooling flows

After a period of major merging at $z \gtrsim 2$ strong, quasi-stationary cooling flows develop at the centers of the clusters despite the strong, super-nova driven energy feedback to the IGM/ICM through galactic super-winds and the use of a fairly top-heavy IMF. As a consequence, stars continue to form steadily at the centers of the cDs ($r \lesssim 10$ kpc) at rates of ~ 100 and $\sim 500 M_{\odot}/\text{yr}$ at $z=0$ for Virgo and Coma, respectively. As discussed in Sommer-Larsen et al. (2005), this results in the cDs becoming too blue over time, with central B-R colours of ~ 1.0 at $z=0$, rather than 1.4-1.5 observed for real cDs (note though that some star-formation is observed in many cDs at the base of the cooling flow — e.g., McNamara 2004). Given the significant gas cool-out rates, the increase in the stellar masses of the cDs since $z \sim 2$ is considerable: For the Virgo cD $M_{*,12}=0.42, 1.0$ and 1.4 in units of $10^{12} M_{\odot}$, at $z=2,1,0$, respectively (inside of 20 kpc). For Coma, the corresponding masses are 0.95, 1.9 and 4.2. In real cDs, the late time cooling flows will be counteracted, most likely by the energy release related to the accretion of mass onto super-massive black holes (e.g., Bower et al. 2006; Croton et al. 2006). This will lead to a strong suppression of the late time star formation rate, such that the simulated cDs become too massive. As will be shown in the next section, the gravitational force of this excess mass influences the central dark matter profile, and must be corrected for.

Assuming that the excess mass has been added adiabatically, i.e. on a timescale large compared to the stellar orbital timescale in the cD, the “correct” dark matter distribution can be recovered by slowly removing the excess stellar mass. This is accomplished as follows:

In order to enable a direct comparison to the observational results obtained for Abell 1703 we focus on dark matter profiles at $z=0.28$, corresponding to $t=10.2$ Gyr. At $t=8.2$ Gyr, stars at $r < 20$ kpc from the center of the cD are identified. For each of the two simulated clusters two additional simulations are carried out — in one the masses of all identified stars formed since $z=1$ are then gradually reduced to zero over a period of 1 Gyr, in the other the masses of all identified stars formed since $z=2$. At the same time radiative cooling as well as star formation is switched off. Subsequently the additional simulations are then continued for 2 Gyrs more, still with radiative cooling and star formation switched off. We refer to these additional simulations as Rz1 and Rz2 respectively.

The purpose of these additional simulations is to, without resorting to completely new simulations with AGN feed-

back etc. included, determine the cluster dark matter profiles in the (more realistic) case where effects of late time cooling flows are counteracted since redshifts of either 1 or 2.

2.2 Dark matter only simulations

To further compliment the existing simulations and determine the role of the inclusion of baryonic physics, we carried out dark matter only simulations of the two clusters using the same initial conditions as previously, but not splitting the particles into SPH and DM particles.

The Virgo and Coma cluster were re-simulated using 1.2 and 4.0 million DM particles, respectively. These simulations will be denoted “VirgoDM” and “ComaDM” in the following. The high resolution DM particles had $m_{DM}=2.6 \times 10^8 h^{-1} M_{\odot}$ and $\epsilon_{DM}=2.8 h^{-1} \text{kpc}$.

Numerical and physical parameters for the simulations and the $z=0$ clusters are summarized in Table. 1

3 RESULTS

3.1 Inner dark matter halo profiles

To enable a precise determination of the galaxy cluster dark matter density profiles at $z=0.28$, 21 time frames, with a time spacing of 0.1 Gyr (large enough to enable quasi-random sampling of the central halo profile) and centered on $t=10.2$ Gyr, were co-added. The DM profile power law index,

$$\alpha(r) = -\frac{d \ln(\rho_{DM}(r))}{d \ln(r)}, \quad (2)$$

where r is the cluster-centric radial distance, was then determined by averaging the co-added DM distribution over spherical shells.

In Fig. 1 is shown by dotted lines the resulting $\alpha(r)$ (strictly speaking $-\alpha(r)$, but we shall neglect this distinction in the following) for the dark matter only simulations. Moreover, $\alpha(r)$ is shown by thick solid curves for the original simulations including baryons, i.e. simulations including baryons, but without any corrections for late cooling-flows and related star formation. Finally, shown by thin solid lines, is $\alpha(r)$ for generalized NFW profiles (eq.[1]) with $\alpha_{NFW}=\alpha(0)=1.09$ and 0.92 , as determined for Abell 1703 by Limousin et al (2008) and Richard et al (2009), respectively, and concentration parameter $c=6$. It is seen from the

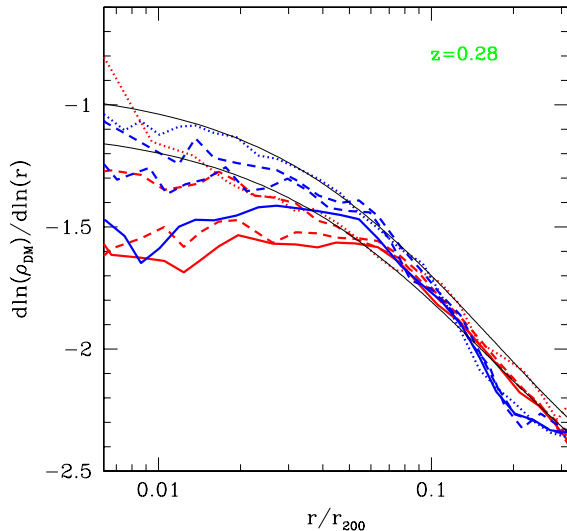


Figure 1. Logarithmic density slopes of the spherically averaged cluster dark matter distributions at $z=0.28$. Solid red curve shows result for the “Virgo” cluster including the cD uncorrected for effects of late time cooling flows. Dotted red curve shows the result of the Virgo DM only simulation. The two red dashed lines show the results of the Rz1 (lower) and Rz2 (upper) re-simulations, where effects of spurious late time cooling flows have been corrected for. The blue curves show the same for the “Coma” cluster. The two black solid curves show generalized NFW models (eq.[1]) with $\alpha_{NFW}=0.92$ (upper) and 1.09 (lower), and concentration parameter $c=r_{200}/r_s=6$.

figure that a) all the simulations match the NFW profiles in the intermediate and outer parts of the haloes, $r/r_{200} \gtrsim 0.07$, fairly well, b) the dark matter only simulation of Virgo is matched quite well by an $\alpha(0) \simeq 1.1$ NFW profile and that of Coma by an $\alpha(0) \simeq 0.9$ profile, and c) the simulations with baryons result in too large values of $\alpha(r)$ ($\sim 1.5 - 1.6$) in the inner parts, $r/r_{200} \lesssim 0.04$ (the results are affected by effects of gravitational softening at $r/r_{200} \lesssim 0.007-0.008$ — see section 3.2.1. for more detail). In order to assess whether this is due to baryonic “over”-pinching, i.e. due to the simulated cDs being unrealistically massive, we compare the simulated and observed Virgo and Coma clusters:

At $z=0$ the cDs in the simulated clusters have masses (inside of $r=50$ kpc — see below) of 7.4×10^{12} and $2.2 \times 10^{12} M_{\odot}$, for Coma and Virgo, respectively (at $z=0.28$ the corresponding numbers are 5.1×10^{12} and $1.8 \times 10^{12} M_{\odot}$). The real Coma and Virgo clusters both contain two dominant galaxies: NGC 4874 and NGC 4889 in Coma, and M86 and M87 in Virgo. The two dominant galaxies in each cluster will eventually merge into one cD in each. The B-band luminosities of NGC 4874 and NGC 4889 are 1.5×10^{11} and $1.8 \times 10^{11} L_{\odot,B}$, respectively (Michard & Andreon 2008). Assuming a B-band M/L of about eight (as found for the cDs in the present simulations based on the Arimoto-Yoshii IMF; the more standard Salpeter IMF results in similar M/L) the combined stellar mass of the two galaxies (at $z \simeq 0$) is $2.6 \times 10^{12} M_{\odot}$. Moreover, the simulated Coma cluster is a $T_X \sim 6$ keV cluster, whereas the real Coma cluster is a

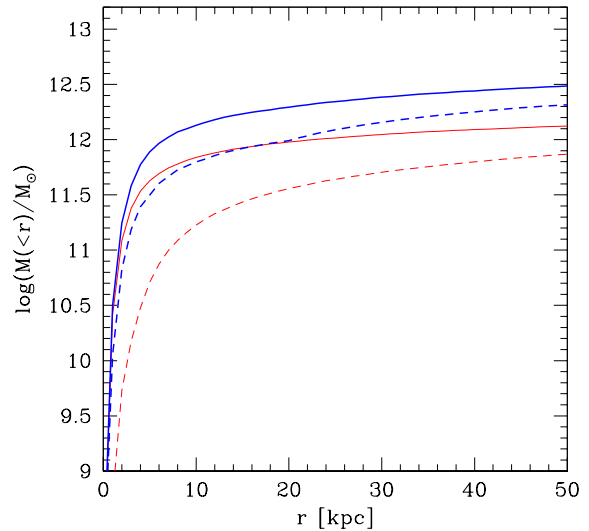


Figure 2. For re-simulations Rz1 (solid curves) and Rz2 (dashed curves), at $z=0$, are shown the cD cumulative stellar masses (Virgo: red curves; Coma: blue curves).

$T_X \sim 8$ keV cluster. Assuming a standard scaling of mass $\propto T_X^{3/2}$ the cD in a 6 keV cluster should have a stellar mass of $1.7 \times 10^{12} M_{\odot}$. The B-band luminosities of M86 and M87 are 4.2×10^{10} and $6.6 \times 10^{10} L_{\odot,B}$, respectively (Binggelli et al. 1985). The stellar masses of the two galaxies thus add up to about $8.6 \times 10^{11} M_{\odot}$.

The simulated cDs are hence about 3-4 times more massive than observed, indicating that the simulated DM haloes are too contracted compared to real ones, which at least qualitatively could explain some of the differences seen in Fig. 1.

To understand the differences seen in Fig. 1 more quantitatively we now turn to the re-simulations aimed at correcting for the effects of the late cooling flows. In Fig. 1 we show by thick dashed lines $\alpha(r)$ for the simulations with baryons, where the mass of all stars in the central cD, formed since either $z_f=1$ or 2, has been adiabatically reduced to zero — we shall denote these two sets of re-simulations by Rz1 and Rz2 in the following. For the inner parts of Coma, a large effect on $\alpha(r)$ results already from removing central stars formed since $z_f=1$. This is related to the fact that the mass of the cD more than doubles since $z=1$ in the original simulation including baryons. For Virgo a strong effect is seen only between the original simulation and $z_f=2$ correction. This is also reasonable, since the mass of the cD more than doubles going from $z=2$ to 1, but then only increases by additional 40% going to redshift 0. In order to assess which of the Rz1 and Rz2 re-simulations, if any, result in cDs which are realistic, we now derive the properties of the resulting cDs.

3.2 Properties of the simulated cD galaxies

3.2.1 cD stellar masses

In Fig. 2 is shown the cumulative stellar mass for the Coma and Virgo cDs from the $z_f=1$ and 2 adiabatically corrected simulations, respectively. It is seen, that at $r=50$ kpc, corresponding to approximately the 25 B-mag/arcsec² (optical) isophote (see below), for $z_f=1$ the cumulative stellar masses are 3.1 and $1.3 \times 10^{12} M_\odot$ for Coma and Virgo, respectively. For $z_f=2$ the corresponding numbers are 2.1 and $0.74 \times 10^{12} M_\odot$. Comparison to the observational estimates above, indicates that the $z_f=2$ cDs provide a better match to reality than the $z_f=1$ ones.

An alternative comparison can be made to the cD of Abell 1703, for which Limousin et al (2008) estimate a stellar mass of $1.3 \pm 0.3 M_\odot$ inside of $r=30$ kpc. The temperature of the Abell 1703 ICM is uncertain, but (also uncertain) estimates of the virial mass of Abell 1703 indicate that the temperature is likely at least as large as for the simulated Coma cluster (Riemer-Sørensen, private communication, Oguri et al 2009). For the Coma Rz1 and Rz2 cDs, at $z=0.28$, we find stellar masses inside of $r=30$ kpc of 2.2 and $1.2 \times 10^{12} M_\odot$. Again, the stellar mass appears realistic for the Rz2 Coma cD, but too large for the Rz1 cD.

3.2.2 cD effective radii

Next, we determine the effective radii for the cDs at $z=0$. To this end, the projected B-band surface brightness profiles are determined for the cDs (see Romeo et al. 2005 for details on calculating broad band photometric properties of the star particles): First, a B-band surface brightness map is constructed by projecting the star-particle distribution within a cube of side-length $L=200$ kpc, centered on the cD, along the three cardinal directions and then superposing the three maps (larger values of L result in similar results). Second, a radial surface profile is constructed by azimuthally averaging over the combined image. Third, the radial profile obtained is divided by a factor of three. At $R \simeq 50$ kpc the B-band surface brightness for both cDs drops to 25 mag/arcsec² (Sommer-Larsen et al. 2005), which is taken to be the radial extent of the cD itself. R_{eff} is then determined as the projected radius enclosing half of the cD B-band luminosity. For the Coma and Virgo cDs in the Rz1 simulations, $R_{\text{eff}}=8$ and 7 kpc is found. The corresponding values for the Rz2 simulations are $R_{\text{eff}}=16$ and 11 kpc. For a large (observational) sample of SDSS galaxies (at $z \sim 0$), Shen et al. (2003) find for early type galaxies of stellar masses 3.1 and $1.3 \times 10^{12} M_\odot$ median effective radii of ~ 25 and 16 kpc, and for stellar masses of 2.1 and $0.74 \times 10^{12} M_\odot$, $R_{\text{eff}} \sim 20$ and 13 kpc. It follows that the Rz1 cDs have too small effective radii for their mass, whereas the Rz2 cDs have reasonable effective radii compared to observations.

3.2.3 cD metal abundances and alpha/Fe ratios

In Fig. 3 is shown, for cDs in the Rz1 and Rz2 re-simulations, the projected average stellar oxygen abundance as a function of projected radius R . In these alpha-element enhanced systems (see below), $[O/H]$ can be taken as a measure of

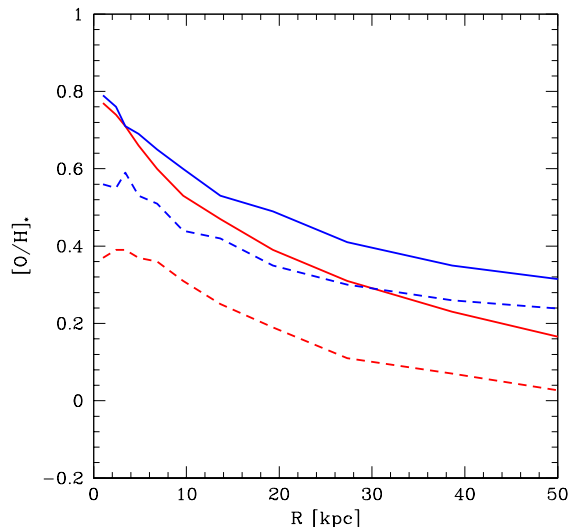


Figure 3. Stellar oxygen abundance as a function of projected radial distance from the center of the cD for re-simulations Rz1 and Rz2, at $z=0$. The curves are labeled as in Fig. 2.

the total abundance $[Z/H]$. It is seen that the oxygen abundance is super-solar all the way to 50 kpc projected radius. For the Rz1 simulations, the integrated (global) cD abundances are $[O/H]=0.59$ for both clusters. For the Rz2 simulations, the integrated abundances are $[O/H]=0.40$ and 0.26 for Coma and Virgo, respectively. Following Thomas et al. (2005), observed early type galaxies of stellar masses 3.1 and $1.3 \times 10^{12} M_\odot$ have median $\langle [Z/H] \rangle = 0.38$ and 0.33 , respectively, and for stellar masses of 2.1 and $0.74 \times 10^{12} M_\odot$, $\langle [Z/H] \rangle = 0.36$ and 0.30 . So the Rz1 cDs have too large abundances compared to what is observed, whereas the Rz2 cDs provide a good match to observations. Taking $[O/Fe]$ as a proxy for alpha/Fe, the results for the Rz1 and Rz2 simulations are similar, $[O/Fe] \sim 0.3-0.35$. These values are within the range observed for large early type galaxies (Thomas et al. 2005).

3.2.4 cD U-V colours

For $z \sim 0$ early type galaxies, the rest-frame U-V broadband colour allows sampling of the 4000 Å break, and therefore is particularly sensitive to age and metallicity variations of the stellar populations. In order to check whether the simulated cDs fall on the observational “red sequence” for early type galaxies, we hence calculate the U-V colours for the cDs. In Fig. 4 is shown, for cDs in the Rz1 and Rz2 re-simulations, the U-V colour as a function of projected radius R . In the inner parts of the galaxies, all the cDs display a negative colour gradient, qualitatively consistent with what is observed for large early type galaxies. As the mean stellar age is approximately constant with projected radius R , the reason for the gradient in colour is the metallicity gradient seen in Fig. 3. This is also the generally accepted explanation for the observed colour gradients in early type systems (e.g. Tamura et al. 2000). For the Rz1 cDs, inte-

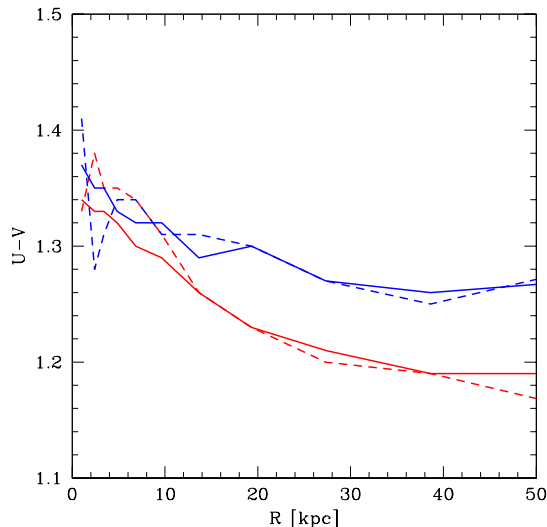


Figure 4. U-V colour as a function of projected radial distance from the center of the cD for re-simulations Rz1 and Rz2, at $z=0$. The curves are labeled as in Fig. 2.

grated (global) U-V colours of 1.31 and 1.27 are found for Coma and Virgo, respectively. For the Rz2 cDs, the corresponding numbers are U-V=1.29 and 1.28. The two Rz1 cDs have $M_V=-24.6$ and -23.7 for Coma and Virgo, respectively. For the Rz2 cDs, the corresponding numbers are -23.8 and -23.0 . Comparing to the observational U-V vs. M_V sequence (e.g. Romeo et al. 2008), early type galaxies of such absolute V magnitudes have a median U-V \sim 1.4. We hence find that the Rz1 and Rz2 cDs have very similar U-V colours, and that these are slightly bluer than the observed average. This is, at least partly, due to the large, somewhat bluer stellar envelope surrounding the cDs, cf. Fig. 4.

3.2.5 cD central physical stellar densities

From the results presented above it is possible to estimate the stellar core density of the cDs, defined as

$$\rho_{c,*} = \frac{M_*(r < R_{\text{eff}})}{4\pi/3 R_{\text{eff}}^3} . \quad (3)$$

For the Rz1 cDs we find $\rho_{c,*}=6$ and $4\times 10^8 M_\odot/\text{kpc}^3$ for Coma and Virgo, respectively. For the Rz2 cDs, the corresponding numbers are 5 and $4\times 10^7 M_\odot/\text{kpc}^3$. Extrapolating the observational estimates of $\rho_{c,*}$, given in van Dokkum et al. (2008) on the basis of SDSS data, to galaxy stellar masses of $\sim 10^{12} M_\odot$, the Rz2 cD core densities appear the most reasonable, although no strong conclusions can be made on the basis of the available data.

3.3 How much are galaxy cluster dark matter haloes pinched by the central cDs?

Based on the results given in the previous subsection, it is clear that the cDs formed in the Rz2 re-simulations give a much better match to reality than the ones formed in the

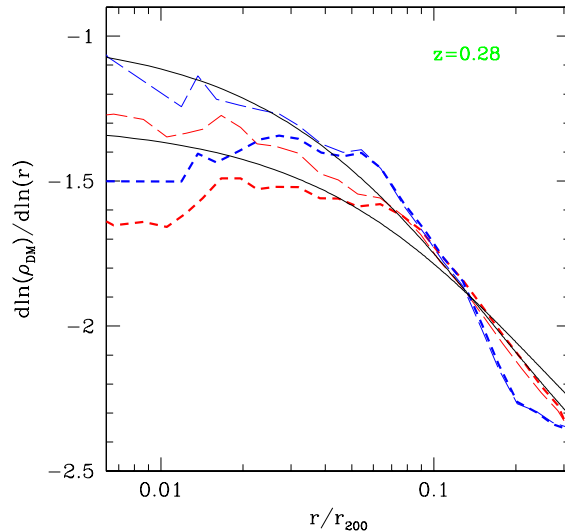


Figure 5. Logarithmic density slopes for the Rz2 re-simulations. Results for total matter densities are shown by thick, short-dashed lines (red: Virgo; blue: Coma). The thin long-dashed lines show the result for the dark matter (as in Fig. 1). The two black solid curves show generalized NFW models (eq.[1]) with $\alpha_{NFW}=1.0$ and 1.3, and concentration parameters $c=r_{200}/r_s=4$ and 6, respectively.

Rz1 simulations, and in fact, in general, meet all observational constraints. We shall hence in the following focus on the Rz2 re-simulations, and the comparison of these to the dark matter only simulations.

3.3.1 Resolution limitations due to gravity softening

The Coma dark matter only simulation has $\epsilon_{\text{DM}}=2.8 h^{-1}\text{kpc}$, and the gravity force of the central dark matter particles is hence purely Newtonian (i.e. un-softened) at $r \simeq 8$ kpc. At $z=0.28$, r_{200} for the Coma cluster is 1820 kpc, which means that the simulation result is affected by resolution effects inside of $r/r_{200} \simeq 0.004$. The Coma simulation with baryons has $\epsilon_{\text{DM}}=5.4 h^{-1}\text{kpc}$, so although the star and gas particle softening lengths are considerably smaller, the resulting dark matter profile may be affected by gravity softening inside of $r/r_{200} \simeq 0.008$. The Virgo simulations with and without baryons have $\epsilon_{\text{DM}}=2.7$ and $2.8 h^{-1}\text{kpc}$, respectively. As r_{200} for this cluster at $z=0.28$ is 1105 kpc, the simulation results may be affected by gravity softening inside of $r/r_{200} \simeq 0.007$. Finally, the VirgoLR simulations have $\epsilon_{\text{DM}}=5.4$ and $5.6 h^{-1}\text{kpc}$, respectively, resulting in an inner radial resolution limit of $r/r_{200} \simeq 0.014$.

In the following we shall only discuss simulation results outside of the above gravity softening resolution limits.

3.3.2 Steepening of the inner dark matter profiles

As can be seen from Fig. 1, the dark matter density profile obtained in the Coma dark matter only simulation, can be fairly well described by a generalized NFW profile of

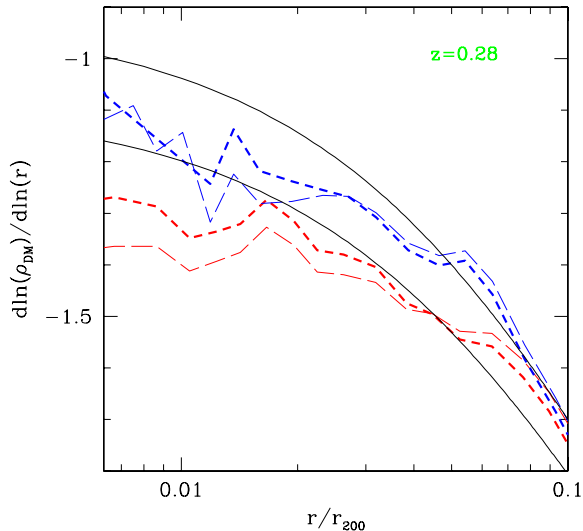


Figure 6. For the Rz2 re-simulations is shown $\alpha(r)$ for the dark matter alone (thick short-dashed lines), and for dark matter and ICM gas combined (thin long-dashed lines). Results for Coma are shown by blue curves, for Virgo by red curves. The two black curves are the NFW models shown in Fig. 1.

$\alpha_{NFW} = \alpha(0) \sim 0.9$. Comparing it to what is obtained for the Rz2 re-simulation of Coma the steepening of the inner dark matter profile, caused by the cD, is quite moderate, $\Delta\alpha \sim 0.1$. For the Virgo cluster, the dark matter only profile is also fairly well described by a generalized NFW profile, this time of $\alpha_{NFW} = \alpha(0) \sim 1.1$. Again, the Rz2 re-simulation only leads to a very moderate steepening, $\Delta\alpha \sim 0.1$, relative to the dark matter only simulation. So for realistic cDs, the steepening of the dark matter profile in galaxy clusters is very moderate, $\Delta\alpha \sim 0.1$. This is the most important result presented in this work.

3.3.3 Total matter density profiles

As gravitational lensing probes the total matter (surface) density, in order to deduce dark matter profiles observationally, one has to do a dark matter vs. baryonic matter decomposition. This obviously adds some uncertainty (statistical as well as possibly systematic) to the estimate of the dark matter density profile. To bypass this, it is clearly also of interest to calculate total matter density profiles from the simulations. These can then more directly be compared to observational finding, based on lensing. In Fig. 5 is shown the result for the Rz2 simulations. Both the Virgo and the Coma profile are characterized by a rather sharp break at $r/r_{200} \simeq 0.05$ - 0.06 . Inside of this the profiles are rather flat, with $\alpha(r) \sim \alpha_{NFW;DM\text{only}} + 0.5$. The profiles are not well described by generalized NFW models, as exemplified in the figure.

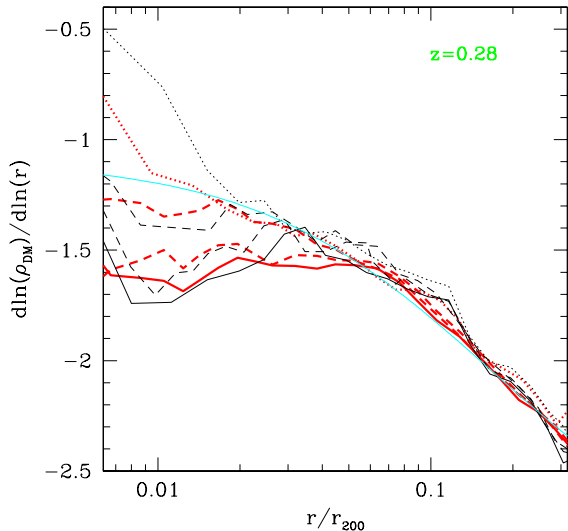


Figure 7. Comparison of the Virgo and VirgoLR simulations, at $z=0$. The red curves display the results for Virgo, labeled in the same way as in Fig. 1. The black curves show the corresponding results for VirgoLR. The statistical uncertainty for the VirgoLR data is $\Delta\alpha \sim 0.05$; for Virgo about a factor of $\sqrt{8}$ less. The light blue curve shows a generalized NFW models (eq.[1]) with $\alpha_{NFW}=1.09$ and concentration parameter $c=r_{200}/r_s=6$.

3.3.4 Dark matter + gas density profiles

In performing the dark matter vs. baryonic matter decomposition mentioned above, one typically assumes that the baryonic component is dominated by the stellar mass of the cD, for which the mass distribution can be fairly well modeled. It is hence important to show, that neglecting the hot gas (ICM) component, for which the mass distribution is much more uncertain, does not significantly bias the estimate of the DM distribution. In Fig. 6 is shown, for the Rz2 simulations, $\alpha(r)$ for the dark matter alone, as well as for dark matter and hot ICM gas combined. As can be seen, the effect on $\alpha(r)$ of including the ICM is very modest, $\Delta\alpha \lesssim 0.05$.

3.4 A numerical resolution test

In Fig. 7 is shown $\alpha(r)$ for the sets of Virgo simulations as well as VirgoLR simulations. Statistical uncertainties on the VirgoLR results are $\Delta\alpha \sim 0.05$, and on the Virgo results about a factor $\sqrt{8}$ less. Note that the VirgoLR results are affected by gravity softening at about $r/r_{200} \simeq 0.014$. Outside of this region, there is reasonably good agreement between the two sets of simulations, indicating that the results presented in Fig. 1 are not seriously affected by numerical resolution limitations outside of $r/r_{200} \simeq 0.007$ - 0.008 .

4 DISCUSSION

Fitting the dark matter density profile of Abell 1703 by a generalized NFW profile, different authors find $\alpha(0)$ between 0.8 and 1.2 (Limousin et al 2008; Saha et al. 2009;

Richard et al 2009; Oguri et al 2009). Although we in this paper are analyzing simulations of just two clusters, and although other observational values of $\alpha(0)$ have previously been reported in the literature, it is obviously interesting that we for the two clusters simulated, including the effects of the central cD on the dark matter halo, find $\alpha(0) \simeq 1.0$ – 1.2 .

Given that LCDM haloes undoubtedly have a range of inner slopes, and given that we are probing only two haloes, an even more interesting result is that for both clusters, the steepening of the inner slopes is both moderate and consistent, $\Delta\alpha \sim 0.1$. For Milky Way sized galaxies, as well as smaller galaxies, Gustafsson et al. (2006) found much larger effects of baryonic pinching of the dark matter haloes, $\Delta\alpha \sim 0.6$. To understand the reason for this difference, we show in Fig. 8, for the Rz2 re-simulations at $z=0.28$, the cumulative masses of dark matter, stars and stars+gas. As can be seen, the cumulative masses of baryons and dark matter are equal at $r_{eq} \simeq 7$ and 9 kpc, for Virgo and Coma respectively. In both cases this is well inside of the effective radius, i.e. the characteristic scale of the galaxy. In contrast, Gustafsson et al. (2006) found $r_{eq} \sim 10$ kpc for the individual (field) galaxies considered. These galaxies have characteristic scales of ~ 2 – 4 kpc, so the chief difference is that the cD galaxies considered in this paper are much less baryon dominated than normal (substantially smaller) field galaxies. In addition, one should note that the present simulations can only probe the increase in dark matter inner profile steepening outside of ~ 8 and 16 kpc, for Virgo and Coma respectively (whereas the innermost, baryon dominated regions are about twice as well resolved due to the shorter gravitational softening lengths of the star and gas particles).

It is also worth noting that Gnedin et al. (2004) found a considerably larger steepening of galaxy cluster inner DM profiles due to baryonic pinching, on the basis of their simulations invoking baryonic physics. This, however (as acknowledged by these authors), is due to the spurious effects of “over-cooling”, discussed and corrected for in the present work.

An underlying assumption in the Rz1 and Rz2 re-simulations is that the rate of change of cD gravitational potential, caused by stars either being formed *in situ* or being added through accretion since $z_f=1$ or 2, is slow (adiabatic), compared to the dynamical rate. Although this is true for the stars forming *in situ* at the base of the cooling flows, in the Coma simulation $\sim 1:3$ and $1:4$ mergers take place at $z \simeq 1.4$ and $z \simeq 0.7$, respectively, and in the Virgo simulation $\sim 1:4$ mergers take place, at $z \simeq 1.5$ and 1.0, respectively. In such mergers, the adiabatic approximation is not fulfilled, and more realistic simulations, including effects of super-massive black hole growth and AGN feedback, would have to be undertaken to check whether the results we find from the adiabatic stellar mass removal re-simulations are in fact fully correct. However, the fact that the Rz2 cDs appear to be realistic in terms of stellar mass, linear extent, metallicity, etc. can be considered very strong evidence that the inner dark matter profile steepening found for the Rz2 simulations are entirely reasonable. It is obvious that the primary drivers of the baryonic pinching are a) cD stellar mass, and, to a lesser extent, b) the cD linear extent.

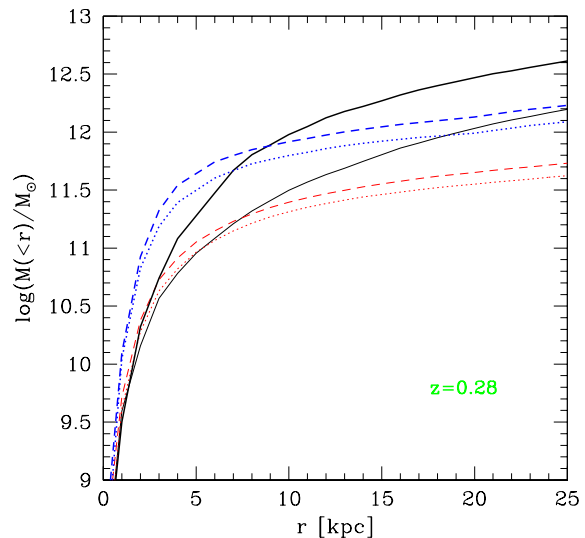


Figure 8. For the Rz2 runs, at $z=0.28$, are shown cumulative mass of dark matter (solid curves; Coma: thick, Virgo: thin), stars (dotted curves; Coma: blue, Virgo: red) and stars+gas (dashed curves; Coma: blue, Virgo: red).

5 CONCLUSION AND OUTLOOK

We have in this paper presented results of cosmological (Λ CDM) TreeSPH simulations of the formation and evolution of two galaxy clusters. In order to quantify the effect of baryonic “pinching” of galaxy cluster dark matter haloes, we have simulated *the same* clusters with and without baryons included.

The hydrodynamical simulations include a number of important physical processes, such as star formation, chemical evolution with non-instantaneous recycling, metallicity dependent radiative cooling, strong star-burst, driven galactic super-winds and the effects of a meta-galactic UV field, including simplified radiative transfer. The two clusters have $T \simeq 3$ and 6 keV, respectively, and both host at $z \sim 0$ a prominent, central cD galaxy.

Comparing the simulations without and with baryons, it is found that for the latter, the inner DM density profiles, $r \lesssim 50$ – 100 kpc, steepen considerably: $\Delta\alpha \sim 0.5$ – 0.6 , where $-\alpha$ is the logarithmic DM density gradient. This is primarily due to the central stellar cDs becoming very massive, as a consequence of the onset of late time cooling flows and related star formation. Once these spurious cooling flows have been corrected for, and the cluster gravitational potentials dynamically adjusted, much smaller pinching effects are found: $\Delta\alpha \sim 0.1$.

The main result of the paper is hence that our work strongly supports the notion that the steepening of the inner dark matter density profile, due to baryonic pinching, is very moderate. This finding is at stark variance with findings for individual field galaxies. The main reason for this is that galaxy clusters, even in the presence of central dominant cD galaxies, are dark matter dominated outside of ~ 7 – 8 kpc. As the effective radii of the two cDs considered are 11 and 16

kpc, this result indicates that cD galaxies are dark matter dominated at the effective radius.

Including the effects of baryonic pinching, central slopes of $\alpha \simeq 1.0$ and 1.2 are found for the DM in the two clusters, interestingly close to recent observational findings for Abell 1703 based on gravitational lensing studies.

For the simulations with baryons, the inner density profile of DM+ICM combined is found to be only very marginally steeper than that of the DM. The total matter inner density profiles, however, are found to be $\Delta\alpha \sim 0.5$ steeper than the inner profiles in the dark matter only simulations. The total matter density profiles are not well described by generalized NFW models.

Given that we have presented results for just two simulated clusters in this paper, it is clearly of importance to increase the sample size. On the observational side, strong lensing constraints for more uni-modal clusters should be obtained. We plan to present such results in forthcoming papers.

ACKNOWLEDGMENTS

We have benefited considerably from discussions with Sune Toft and Signe Riemer-Sørensen. We gratefully acknowledge abundant access to the computing facilities provided by the Danish Centre for Scientific Computing (DCSC). This work was supported by the DFG Cluster of Excellence ‘‘Origin and Structure of the Universe’’. The Dark Cosmology Centre is funded by the Danish National Research Foundation. ML acknowledges the Centre National d’Etudes Spatiales (CNES) for their support.

REFERENCES

- Allen, S. W., Edge, A. C., Fabian, A. C., et al. 1992, MNRAS, 259, 67
- Arabadjis, J. S., Bautz, M. W., & Garmire, G. P. 2002, ApJ, 572, 66
- Austin, C. G., Williams, L. L. R., Barnes, E. I., Babul, A., & Dalcanton, J. J. 2005, ApJ, 634, 756
- Binggelli, B., Sandage, A., & Tammann, G. A. 1985, AJ, 90, 1681
- Biviano, A. & Salucci, P. 2006, A&A, 452, 75
- Blumenthal, G. R., Faber, S. M., Flores, R., & Primack, J. R. 1986, ApJ, 301, 27
- Bower R.G., Benson A.J., Malbon R., Frenk C.S., Baugh C.M., Cole S., Lacey C.G. 2006, MNRAS 370, 645
- Bradač, M., Schrabback, T., Erben, T., et al. 2007, ArXiv e-prints, 0711.4850
- Böhringer, H., Voges, W., Huchra, J. P., et al. 2000, ApJS, 129, 435
- Cleary, P. W., & Monaghan, J. J., 1999, Journal of Computational Physics, 148, 227
- Croton, D.J., et al. 2006, MNRAS, 367, 864
- Dahle, H., Hannestad, S., & Sommer-Larsen, J. 2003, ApJL, 588, L73
- D’Onghia, E., Sommer-Larsen, J., Romeo, A. D., Burkert, A., Pedersen, K., Portinari, L., & Rasmussen, J. 2005, ApJL, 630, L109
- El-Zant, A., Shlosman, I., & Hoffman, Y. 2001, ApJ, 560, 636
- El-Zant, A. A., Hoffman, Y., Primack, J., Combes, F., & Shlosman, I. 2004, ApJL, 607, L75
- Elíasdóttir, Á., Limousin, M., Richard, J., et al. 2007, ArXiv e-prints, 0710.5636
- Ettori, S., & Fabian, A.C., 2000, MNRAS, 317, 57
- Ettori, S., Fabian, A. C., Allen, S. W., & Johnstone, R. M. 2002, MNRAS, 331, 635
- Gao, L., Navarro, J. F., Cole, S., et al. 2008, MNRAS, 387, 536
- Gavazzi, R. 2005, A&A, 443, 793
- Gavazzi, R., Fort, B., Mellier, Y., Pelló, R., & Dantel-Fort, M. 2003, A&A, 403, 11
- Ghigna, S., Moore, B., Governato, F., et al. 2000, ApJ, 544, 616
- Gnedin, O. Y., Kravtsov, A. V., Klypin, A. A., & Nagai, D. 2004, ApJ, 616, 16
- Gustafsson, M., Fairbairn, M., & Sommer-Larsen, J. 2006, Ph.Rev.D., 74, 123522
- Haardt, F., & Madau, P. 1996, ApJ, 461, 20
- Hansen, S. H. & Stadel, J. 2006, Journal of Cosmology and Astro-Particle Physics, 5, 14
- Kay, S. T., Pearce, F. R., Frenk, C. S., & Jenkins, A., 2002, MNRAS, 330, 113
- Kazantzidis, S., Magorrian, J., & Moore, B. 2004, ApJ, 601, 37
- Kelson, D. D., Zabludoff, A. I., Williams, K. A., et al. 2002, ApJ, 576, 720
- Kneib, J., Hudelot, P., Ellis, R. S., et al. 2003, ApJ, 598, 804
- Lewis, A. D., Buote, D. A., & Stocke, J. T. 2003, ApJ, 586, 135
- Lia, C., Portinari, L., & Carraro, G. 2002a, MNRAS, 330, 821
- Lia, C., Portinari, L., & Carraro, G. 2002b, MNRAS, 335, 864
- Limousin, M., Richard, J., Jullo, E., et al. 2007b, ApJ, 668, 643
- Limousin, M. et al 2008, A&A, 489, L23
- Ma, C.-P. & Boylan-Kolchin, M. 2004, Physical Review Letters, 93, 021301
- Mandelbaum, R., Seljak, U., & Hirata, C. M. 2008, ArXiv e-prints, 0805.2552
- Michard, R., & Andreon, S. 2008, A&A, 490, 923
- Moore, B., Governato, F., Quinn, T., Stadel, J., & Lake, G. 1998, ApJL, 499, L5
- Muanwong, O., Kay, S. T., & Thomas, P. A., 2006, ApJ, 649, 640
- Navarro, J. F., Frenk, C. S., & White, S. D. M. 1997, ApJ, 490, 493
- Navarro, J. F., Hayashi, E., Power, C., et al. 2004, MNRAS, 349, 1039
- Nipoti, C., Stiavelli, M., Ciotti, L., Treu, T., & Rosati, P. 2003, MNRAS, 344, 748
- Nipoti, C., Treu, T., Ciotti, L., & Stiavelli, M. 2004, MNRAS, 355, 1119
- Oguri, M., et al. 2009, ApJ, submitted (astro-ph/0901.4372)
- Okabe, N., et al. 2009, ApJ, submitted (astro-ph/0903.1103)
- Orban de Xivry, G. & Marshall, P., 2009, MNRAS, sub-

- mitted (astro-ph/0904.1454)
- Pointecouteau, E., Arnaud, M., & Pratt, G. W. 2005, *A&A*, 435, 1
- Richard, J., Kneib, J.-P., Jullo, E., et al. 2007, *ApJ*, 662, 781
- Richard, J., Pei, L., Limousin, M., Jullo, E., & Kneib, J. 2009, *A&A*, in press (astro-ph/0901.0427)
- Ricotti, M. 2003, *MNRAS*, 344, 1237
- Riemer-Sørensen, S., Paraficz, D., Ferreira, D. D. M., Pedersen, K., Limousin, M. & Dahle, H. 2009, *ApJ*, 693, 1570
- Romeo, A. D., Portinari L., & Sommer-Larsen, J. 2005, *MNRAS*, 361, 983
- Romeo, A. D., Sommer-Larsen, J., Portinari, L., & Antonuccio-Delogu, V., 2006, *MNRAS*, 371, 548
- Romeo, A. D., Napolitano, N. R., Covone, G., Sommer-Larsen, J., Antonuccio-Delogu, V., & Capaccioli, M. 2008, *MNRAS*, 389, 13
- Sand, D. J., Treu, T., & Ellis, R. S. 2002, *ApJL*, 574, L129
- Sand, D. J., Treu, T., Ellis, R. S., Smith, G. P., & Kneib, J.-P. 2008, *ApJ*, 674, 711
- Sand, D. J., Treu, T., Smith, G. P., & Ellis, R. S. 2004, *ApJ*, 604, 88
- Saha, P. & Read, J. I. 2009, *ApJ*, 690, 154
- Saro A., Borgani S., Tornatore L., Dolag K., Murante G., Biviano A., Calura F., & Charlot S., 2006, *MNRAS* 373, 397
- Shen, S. et al. 2003, *MNRAS*, 343, 978
- Smith, G. P., Kneib, J.-P., Ebeling, H., Czoske, O., & Smail, I. 2001, *ApJ*, 552, 493
- Smith, G. P., Kneib, J.-P., Smail, I., et al. 2005, *MNRAS*, 359, 417
- Sommer-Larsen J., Götz M., Portinari L., 2003, *ApJ*, 596, 46
- Sommer-Larsen J., Romeo, A. D., Portinari L., 2005, *MNRAS*, 357, 478
- Springel, V., & Hernquist, L., 2002, *MNRAS*, 333, 649
- Tamura, N., Kobayashi, C., Arimoto, N., Kodama, T. & Ohta, K. 2000, *AJ*, 119, 2134
- Thomas, D., Maraston, C., & Bender, R. 2005, *ApJ*, 621, 673
- Thomas, P. A., , Muanwong, O., Kay, S. T., & Liddle, A. R., 2002, *MNRAS*, 330, L48
- Tornatore, L., Borgani, S., Matteucci, F., Recchi, S., & Tozzi, P., 2004, *MNRAS*, 349, L19
- Tornatore, L., Borgani, S., Dolag, K., & Matteucci, F. 2007, *MNRAS*, 382, 1050
- Tyson, J. A., Kochanski, G. P., & dell'Antonio, I. P. 1998, *ApJL*, 498, L107
- Valdarnini, R., 2003, *MNRAS*, 339, 1117
- van Dokkum, P. G., et al. 2008, *ApJL*, 677, L5
- Zappacosta, L., Buote, D. A., Gastaldello, F., et al. 2006, *ApJ*, 650, 777